PASJ: Publ. Astron. Soc. Japan **64**, 46, 2012 June 25

Standing Kink Waves with Longitudinal Flow in Fine Threaded Coronal Loops: A New Method for the Coronal Seismology through Beat and Damped Waves

Vinay Shankar PANDEY, Tetsuya MAGARA, and Dong-Hun LEE
School of Space Research, Kyung Hee University, Yongin, Gyeonggi-Do, 446-701, Korea
vspandey@khu.ac.kr, magara@khu.ac.kr, dhlee@khu.ac.kr

(Received 2011 August 16; accepted 2011 November 16)

Abstract

Stimulated by the first weakly attenuated standing kink oscillations of coronal fine threads filled with cool flowing plasma, seen in a recent Ca II H-line observed by Solar Optical Telescope (SOT) aboard Hinode, in this study we present the effects of longitudinal flow on the standing wave. We have found that flow generates two important consequences: first, it produces a frequency shift, which leads to the phenomenon of wave beating; second, it splits the damping time of the forward and backward waves of the attenuated standing wave (considered here only the resonance absorption) into two different values. A comparative analysis of the beat waves, within the "quarter-beat period approximation" together with attenuated waves, seems to be very appealing for coronal seisomology. We refer a new parameter, modulating time ($\tau_{\rm m}$), which is defined as the time when the amplitude of the beat wave becomes zero for a wave train that lies within a quarter period of the beat envelope, the so-called "quarter beat period approximation". We can compare this $\tau_{\rm m}$ with the attenuating time ($\tau_{\rm D}$) to discriminate the behaviour of the signal, as follows: if $\tau_{\rm m} > \tau_{\rm D}$, the envelope of the signal is dominated by attenuation due to resonance absorption, while if $\tau_{\rm m} < \tau_{\rm D}$, the envelope of the signal is dominated by modulation due to beating. Since observation corresponds to first inequality, the amplitude of the signal seems to be dominated by attenuation due to resonance absorption. Hence, the inequality $\tau_{\rm m} \geq \tau_{\rm D}$ imposes an upper bounds for the density contrast and magnetic field for a given value of the observed flow. Besides these, we also find that the flow-generated splitting of the damping time also leads to an $\sim$8%–10% uncertainty in our estimation of the radial inhomogeneity across the loop boundary, as compared to the static case, i.e., when the flow is zero.

Key words: Sun: corona — Sun: MHD waves, coronal-seismology

1. Introduction

The existence of flows has been revealed in space and solar plasmas almost on all spatial and temporal scales by present-day high-resolution observations. They are almost ubiquitous in virtually all active region loops, where most of the wave activities take place. Flows play an important role in modifying the frequency of waves. This modification has been exploited in helioseismology to measure various transverse flow velocities (with respect to the line of sight), like solar rotation and meridional flow at different depths beneath the photosphere (Thompson et al. 1996; Basu et al. 1999; Antia et al. 2008). A similar application to coronal seismology is possible, but has not been reported so far. In this work, we show that the existence of flow precludes the existence of standing waves in the strictest sense. However, for small values of flow, we can obtain modulated standing waves with a slowly varying amplitude in the temporal-domain, as was demonstrated recently by Terradas, Goossens, and Ballai (2010a). We discuss this result in relation to the recent Hinode (Solar Optical Telescope: SOT) observations of standing waves (Ofman & Wang 2008) in thin coronal threads, and arrived at a very stringent value of the physical parameter on the basis of wave measurements.

Coronal seismology is a new tool to diagnose the physical parameters of coronal loops. It was first developed by Uchida (1970), followed by Roberts, Edwin, and Benz (1984), in the context of coronal loops. This method was recently applied to various data from Solar and Heliospheric Observatory (SOHO), Transition Region And Coronal Explorer (TRACE), and Hinode (e.g., Nakariakov et al. 1999; Ofman & Wang 2002; Verwichte et al. 2004; Ofman 2007; Wang et al. 2007; Van Doorsselaere et al. 2007, 2008b; Ofman & Wang 2008; Gruszecki et al. 2008).

Omnipresent small-amplitude waves observed in the corona by Tomczyk et al. (2007) using the Coronal Multi-channel Polarimeter (CoMP) were identified as fast magneto-acoustic kink waves (Van Doorsselaere et al. 2008a). Further, Van Doorsselaere et al. (2008b) reported the first spectroscopic detection of kink magnetohydrodynamic (MHD) oscillation of a solar coronal structure by Extreme-ultraviolet Imaging Spectrometer (EIS) aboard the Japanese Hinode satellite. They reported the amplitude of oscillations to be $\approx 1\,{\rm km\,s^{-1}}$ in the Doppler shift of the Fe XII 195 Å spectral line (1.3 MK). The unique simultaneous imaging and spectroscopic capabilities of EIS allow one to measure both the loop length and the density, which are the essential parameters for estimating the coronal magnetic field. Therefore, with the observed value of the period (P) of the kink oscillation, one can easily calculate the magnetic field by using the following well-known relation: $B = 2L\sqrt{2\pi n m_{\rm p}}/P$, where L, n, and $m_{\rm p}$ are the loop length, electron density, and proton mass, respectively. This first spectroscopic detection of kink waves in a coronal magnetic structure does not give any evidence of background plasma flows. However, the recent discovery by Ofman and

Wang (2008) of the SOT/Hinode observation shows a transient flow in the plane-of-sky as an apparently field-aligned displacement of the emission brightness. This can be interpreted as a flow; however, there may be other possible interpretations, e.g., thermal and/or ionisation fronts, which cannot be ruled out. We interpret the observed field-aligned displacement of the emission brightness in terms of flow. The cool chromospheric material appears to flow along the thin threads with an average speed that lies in the range of 74–123 km s^{-1}. The existence of a million-degree plasma within the loop was confirmed by low-resolution (3″) observations of the same region in the Fe XII 195 Å line by SOHO/EIT. Ofman and Wang (2008) suggested that a flare preceding the oscillation might have been responsible for filling some of the threads of the loop with flowing chromospheric material visible in the Ca II H line.

The SOT observations have a much higher spatial resolution than EIS. Thus, the observation by Ofman and Wang (2008) of chromospheric material flowing along very narrow coronal structures provides us with an unique opportunity to model the oscillations of cool (10000 K–20000 K) threads embedded in hot (1 MK) plasma. The density of the flowing gas is an unknown parameter, because it depends on the amount of chromospheric material that is injected into the thread. We will examine the dispersion relation for magnetoacoustic modes of a cylinder and discuss the consequences of the modification of the frequency due to the introduction of the flow. It is noted that although slow body waves are also solutions of the dispersion relation [for more clarification see Edwin and Roberts (1983)], the associated periods are many times larger than the observed period. We thus focus our attention on fast body waves, particularly on fast mode-standing kink waves in this present work. It also looks essential to give a few sentences about the differences between standing and propagating kink waves. For that we reiterate the arguments of Terradas, Goossens, and Verth (2010b), that standing transverse osscillations are the result of an initial-value problem in which an initial disturbance in the solar corona due to solar flare or CME induces oscillations in the coronal loops at their natural frequencies, or eigen modes. In the initial-value problem the wavenumber is fixed, and the system chooses the proper frequency to accommodate the kink mode in the tube. Contrary to the standing oscillation of the initial-value problem, the transverse propagating waves have a forced nature in which photospheric motion acts as a driver, as for example the frequencies of the kink waves observed by CoMP show a peak at around 5 min, revealing a possibility of a p-mode driven photospheric origin. However, this is just a possibility it may be connected with the characteristic time of the granulation, which is about 10 min.

Moreover, in the driven problem, the frequency is fixed, but the system chooses the proper wavelength (along the waveguide) to accommodate the kink mode in the tube (e.g., Terradas et al. 2010b). The aim of this paper is to develop the work of Terradas, Goossens, and Ballai (2010a), making a comparative parametric study of the modulated and attenuated signals. Specifically, we address the following issues concerning coronal seismology: precise estimations of the density contrast, magnetic field, and radial inhomogeneity length-scale across the loop boundary by applying the present developed method on recent observational data of SOT/Hinode, which detected weakly attenuated coronal loop oscillations in the presence of background flow (e.g., Ofman & Wang 2008). The dispersion relation is presented in section 2, results in section 3, while these results are discussed in section 4 along with the major conclusions.

2. Model and Dispersion Relation

2.1. *Estimation of the Modified Frequency/Period in Presence of Flow*

We consider a cylinder model of the loop, as illustrated in figure 1, and use the dispersion relation of Narayanan (1991) and Goossens, Hollweg, and Sakurai (1992), which is summarized here. We consider both the equilibrium magnetic field, $\boldsymbol{B}_0$, and steady flows i.e., $V_0 = U_i$ to be directed parallel to the axis of a cylindrical tube (z-axis) of radius "R". We assume $k = \pi/L$, in accordance with the length scale, L, of the observed disturbance. We denote region 1 as $|r| > R$, and region 2 as $|r| < R$, and assume that the equilibrium state of the plasma is uniform in regions 1 and 2. The flow speed, U_i, with $i = 1, 2$ corresponds to flow in regions 1 and 2. However, in this work, we assume $U_2 = U$ and $U_1 = 0$ as a special case. We consider the propagation vector $\boldsymbol{k} = k\hat{z}$ and the magnetic field $\boldsymbol{B}_0 = B_0\hat{z}$ to be in the z-direction. In this case, the $\hat{r}$-direction is normal to both the propagation vector and the background magnetic field. We consider perturbations of the following form: $f(r)\exp i(-kz)\ \exp[i(\omega t + n\theta)]$, with $n = 1$ corresponding to the kink mode. It can be shown that the radial dependence of the flow variables satisfies the modified Bessel differential equation. By simple algebraic manipulation, the dispersion relation can be shown to be (Narayanan 1991; Goossens et al. 1992)

$$\rho_{02}(k^2v_{\rm A2}^2 - \Omega^2)m_1F_n(m_1, m_2, R) - \rho_{01}(k^2v_{\rm A1}^2 - \Omega^2)m_2 = 0, \quad (1)$$

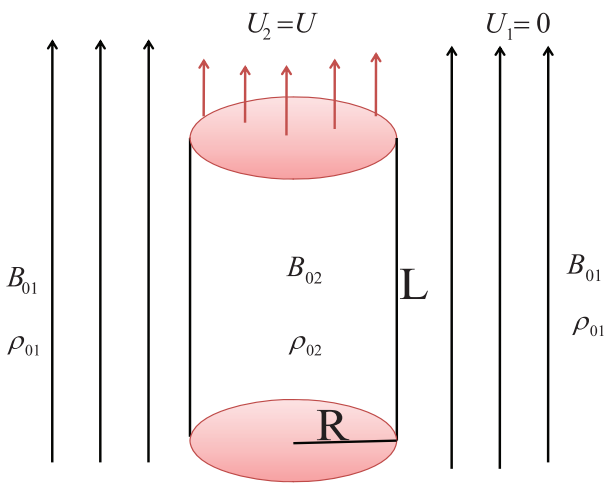

Fig. 1. Scratch of the cylinder model of the loop of length L and radius R. The region occupied by the loop is denoted as region 2 while the region outside the loop is represented by region 1. The magnetic field and flow are directed along the axis of the loop that is along the z-direction.

where $\Omega = \omega - kU_i$ is the Doppler-shifted frequency and

$$m_i^2 = \frac{(c_{si}^2 k^2 - \Omega_i^2)\ (v_{Ai}^2 k^2 - \Omega_i^2)}{(c_{si}^2 + v_{Ai}^2)\ (c_{Ti}^2 k^2 - \Omega_i^2)}, \tag{2}$$

$$F_n(m_1, m_2, R) = \frac{I_n(m_2 R) K_n^{'}(m_1 R)}{I_n^{'}(m_2 R) K_n(m_1 R)} \tag{3}$$

with

$$c_{si}^2 = \gamma p_{0i}/\rho_{0i},\ v_{Ai}^2 = B_{0i}^2/4\pi\rho_{0i} \tag{4}$$

and

$$c_{Ti}^2 = c_{si}^2 v_{Ai}^2/c_{si}^2 + v_{Ai}^2. \tag{5}$$

I_n and K_n denote the modified Bessel function of order n. In the above equations, a prime ($'$) denotes the derivative of the Bessel function, e.g., $I_n^{'}(m_2 a) \equiv \frac{d}{dz} I_n(z)$ evaluated at $z = m_2 R$. In the absence of background flow, $U = 0$, which implies $\Omega = \omega$, the dispersion relation (1) reduces to the Edwin and Roberts (1983) dispersion relation (8). We can distinguish the trapped surface and body waves as follows:
(i) if m_1^2 and $m_2^2 > 0$, then we have surface waves,
(ii) if $m_1^2 > 0$ and $m_2^2 < 0$, then we have body waves.

Recently, Vasheghani Farahani et al. (2009) have adopted this theoretical model of the MHD mode guided by a field-aligned plasma cylinder with a steady flow to study transverse waves observed in solar coronal hot jets, discovered with Hinode/XRT. Their study is basically concerned about the propagating fast magnetoaoustic kink waves. However, since the observation of Ofman and Wang (2008) reveals standing waves, therefore in our present study we apply this theoretical model on the standing kink waves in the presence of steady flow. In a thin tube, the TT-approximation ($kR \ll 1$) above the dispersion relation (1) yields a modified frequency of the kink wave due to internal flow along the thread, as follows [cf. equation (70) of Goossens et al. (1992)]:

$$\omega_{kf} = k\frac{\rho_{02} U}{\rho_{01} + \rho_{02}} \pm \omega_{cm}, \tag{6}$$

where ω_{kf} is the flow effected kink frequency, and ω_{cm} is the frequency in the centre-of-mass frame suggested by Hollweg et al. (1990),

$$\omega_{cm}^2 = \omega_k^2 - \frac{\rho_{01}\rho_{02}}{(\rho_{01} + \rho_{02})^2} k^2 U^2, \tag{7}$$

where ω_k is the kink frequency without flow defined as follows:

$$\omega_k^2 = \frac{\rho_{01}\omega_{A1}^2 + \rho_{02}\omega_{A2}^2}{(\rho_{01} + \rho_{02})}, \tag{8}$$

with ω_{Ai}, $i = 1, 2$ corresponds to local Alfvén frequency.

Recently Terradas, Goossens, and Ballai (2010a) have further approximated the above equations (6)–(8) in terms of a linear relation that defines the modified kink wave frequency as a funtion of flow [their equation (17)]:

$$\omega_{kf\pm} = \omega_k \left[1 + x\frac{\rho_{02}}{(\rho_{01} + \rho_{02})}\right], \tag{9}$$

with $x = kU/\omega_k$, and under the condition of slow flow i.e., $U/v_A \ll 1$, which corresponds to $x \ll 1$. This equation (9) is very useful to explain the phenomenon of wave beating of the standing wave due to flow. More details about this are discussed in the following subsequent section.

2.2. *Estimation of the Damping Time by Using the Thin Tube Thin Boundary (TTTB) Approximation, i.e., Resonance Absorption*

Damping of the kink MHD waves by resonant absorption can be achieved by introducing additional physics in the equlibrium model of a uniform cylinder. The required additional physics is the radial non-uniformity of the local Alfvén velocity in the thin boundary (TB) layer across the loop. For a constant magnetic field this can be accommodated by a radial non-uniform density (e.g., Goossens et al. 2008). The studies related to a smooth nonuniformity of the transverse-characteristic speeds across the loop boundary and associated mechanism for the kink MHD waves damping "resonance absorption" have been widely discussed by many earlier workers (e.g., Goossens et al. 1992; Ruderman & Roberts 2002; Goossens et al. 2008). It should be evident that the mechanism of the resonant absorption appears only in the case of the smooth transverse nonuniformity. On the other hand, the physical parameters in the loop can well be constant, and experience a steep jump at its transverse boundary. Moreover, kink modes can exist even when there are no non-uniformities of the characteristic speeds across the magnetic field at all, by reflection on the tangential discontinuities of the plasma flows (cf. Nakariakov et al. 1996). In a non-uniform tube the frequency of the wave becomes complex (e.g., $\omega = \omega + i\gamma$) due to mode conversion at the inhomogeneous layer; an inverse of the imaginary part of the frequency yields the associated damping time. The complete derivation of the damping rate (γ), taking into account the effect of longitudinal flows, is extensively given in Goossens, Hollweg, and Sakurai (1992) [cf. their equation (76)], so we do not repeat it again; interested readers are urged to refer the original paper. Recently, Terradas, Goossens, and Ballai (2010a) have further simplified the damping-rate expression of Goossens, Hollweg, and Sakurai (1992), in terms of a linear approximate relation [e.g., their equation (28)] for the sinusoidal density and flow profiles inside the loop. One novelty of their expression is that it gives very accuate results compared to numerical calculations of the full resistive eigen-value problem. In our analysis, we also borrow their expression (28) to calculate the damping rate in the presence of flow, as follows:

$$\gamma_\pm = -\frac{1}{4}\frac{l}{R}\frac{(\rho_{02} - \rho_{01})}{(\rho_{02} + \rho_{01})}\omega_k \times \left\{1 \pm \frac{kU}{\omega_k}\left[-\frac{8\rho_{01}\rho_{02}}{(\rho_{02}^2 - \rho_{01}^2)} - \frac{(\rho_{02} - \rho_{01})}{(\rho_{02} + \rho_{01})} + \frac{(\rho_{02} + \rho_{01})l}{(\rho_{02} - \rho_{01})l^*}\right]\right\}, \tag{10}$$

where the $\pm$ sign corresponds to the forward and backward waves of the standing waves travelling in opposite directions; the other symbols have their usual meaning, as given in Terradas, Goossens, and Ballai (2010a). We can easily visualize from equation (10) that the flow splits the damping rate, and both the forward and backward waves have distinct rates. In general, an arbitrary initial perturbation excites both forward and backward propagating waves at the same time. As a result, the system will oscillate as a combination of these two waves

with two different "e-folding" envelopes, which can be understood as follows: $\sin(kz)[\cos(\omega_{\rm f}t)e^{-\gamma_1 t} + \cos(\omega_{\rm b}t)e^{-\gamma_2 t}] - \cos(kz)[\sin(\omega_{\rm f}t)e^{-\gamma_1 t} - \sin(\omega_{\rm b}t)e^{-\gamma_2 t}]$, where, $\omega_{\rm f} = \omega_0 + \Delta\omega$ and $\omega_{\rm b} = \omega_0 - \Delta\omega$ are flow-generated frequency shifts corresponding to the forward and backward waves, and γ_1 and γ_2 are flow-generated splittings of the damping rates. The above combination can be expressed in terms of pure damped standing waves, i.e., $\sin(kz)\cos(\omega t)e^{-\gamma t}$, only when $\omega_{\rm f} = \omega_{\rm b} = \omega$ and $\gamma_1 = \gamma_2 = \gamma$. Consequently, we can say that it is mathematically not possible to set up pure damped standing waves in presence of flows with a unique value of the damping rate. In other words, in terms of standing waves we can say that the flow splits the damping rate of the standing waves, and hence its forward component would attain a different damping rate as compared to the backward component. This splitting also affects the estimation of the radial inhomogeneity length scale across the loop boundary. More details about this will be discussed in the subsequent section below.

3. Results

As discussed above, since in this paper we are interested in the fast mode kink waves, in our analysis we consider only $n = 1$ in the dispersion relation (1), just to follow the observational findings of Ofman and Wang (2008). We solved the dispersion relation numerically, and coded it in MATLAB. The dispersion relation (1) describes the functional dependence of the frequency, ω, on the wavenumber, k, which can be utilized for both standing and propagating waves. For the case of the standing-wave axial wavelength (or axial wavenumber k) is specified and the dispersion relation is solved for the frequency ω. However, for the case of a propagating wave, a wave generated at a given location with a specified frequency, ω, is considered, and the dispersion relation is solved for the wavenumber k; for more details see Terradas, Goossens, and Verth (2010b). The effect of compressibility, flows, and magnetic-field gradients on surface waves in slab Narayanan (1990) and cylindrical geometry Narayanan (1991) have already been studied in detail. Also, in this study we assume the plasma beta to be small.

A recent observation by Ofman and Wang (2008) suggests that the fine threads are clearly marked in coronal loops due to chromospheric material flowing along the threads. Threads are less than 0.″5 wide, and the average flows of the chromospheric material were found to be in the range of $\sim$74–123 km s^{-1}. We modeled region 1 corresponding to loops suggested by Ofman and Wang (2008), using the SOHO/EIT 195 Å observations of the same active region in much lower resolution of (3″), which confirmed the presence of coronal loops at that moment. We considered the typical coronal loop parameters, namely its loop length, 70 Mm; density, $n_{01} = 2 \times 10^9$ cm^{-3}; temperature, $T_{01} = 1 \times 10^6$ K; magnetic field, B_{01} in the range of 20–50 G. However, for region 2 we considered the temperature, $T_{02} = 2 \times 10^4$ K for the chromospheric material. Since the cool chromospheric material is observed to be flowing along the identified coronal loops structure, we considered the magnetic field strength of the thin threads (region 2) to be equal to coronal field strengths (region 1). The most uncertain physical parameter related to the thread is its density, because it originates due to an impulsive event (flare) that occurs in the vicinity of the observed loop footpoints. On the other hand, the magnetic field may not be much different from the value extrapolated from the photosphere.

3.1. *Modulation of Standing Waves in Coronal Structures with Flow: Phenomenon of Wave Beating*

In all of the previous studies concerning the effect of flow on the frequency of the waves in an inhomogeneous plasma, it was reported that the flow will produce a negligible shift of the frequency if the flow speed is very small compared to the phase speed of the waves (Nakariakov & Roberts 1995). For the observations under discussion, the flow speeds are indeed small compared with the phase speeds of the forward and backward waves of the standing wave. It should be noted that for the static case (i.e., no flow), both the forward and backward waves of the standing wave propagate with the same phase speed. However, in the considered case with flow, those phase speeds are different. A modification of the period of oscillation by the flow leads to an interesting phenomenon related to standing waves. In the absence of any flow, a standing wave is set up when waves of equal amplitude, moving along opposite directions, combine together to produce a pattern of nodes and anti-nodes that are fixed in space. The phase of the standing wave will be solely a function of space. A node consisting of a trough will always remain a trough, while an anti-node consisting of a crest will always remain a crest. In the presence of a flow, the oscillation period for a wave moving along the flow will be different from the period of the wave that moves anti-parallel to the flow. Let $\Delta\omega$ be the difference in the frequency of waves that are parallel and anti-parallel to the flow. For our dispersion relation, the frequency of anti-parallel flow was found to be smaller than frequency of parallel flow. Thus, $\Delta\omega$ would be positive. Since the axial wavenumber (k) is fixed for the standing wave, the well-known dispersion relation given in equation (6) yields two different frequencies in presence of flow. Consequently, the standing wave can be expressed as a superposition of two waves (e.g., forward and backward), as follows:

$$f = x_{\rm f0}\sin[(kz - \omega_{\rm f}t)] + x_{\rm b0}\sin[(kz + \omega_{\rm b}t)], \tag{11}$$

where

$$\omega_{\rm f} = kc_{\rm k}\sqrt{1 - \frac{\rho_{01}\rho_{02}}{(\rho_{01}+\rho_{02})^2}\frac{U^2}{c_{\rm k}^2}} + \frac{\rho_{02}}{(\rho_{01}+\rho_{02})}kU \tag{12}$$

and

$$\omega_{\rm b} = kc_{\rm k}\sqrt{1 - \frac{\rho_{01}\rho_{02}}{(\rho_{01}+\rho_{02})^2}\frac{U^2}{c_{\rm k}^2}} - \frac{\rho_{02}}{(\rho_{01}+\rho_{02})}kU. \tag{13}$$

When the transverse displacements of the tube axis for both waves are equal, i.e., $x_{\rm f0} = x_{\rm b0} = x_0$, which corresponds to the case of perfect reflection from the node points, we can write equation (11) as

$$f = x_0[\sin(kz - \omega_{\rm f}t) + \sin(kz + \omega_{\rm b}t)] \tag{14}$$

or

$$f = x_0 \{\sin(kz)\,[\cos(\omega_f t) + \cos(\omega_b t)] - \cos(kz)\,[\sin(\omega_f t) - \sin(\omega_b t)]\}. \quad (15)$$

This equation (15), which is analogous to equation (30) of Terradas, Goossens, and Ballai (2010a), reveals that pure standing waves can be obtained only in the absence of flow, i.e., for the situation of $\omega_f = \omega_b$. In other words, we can say that mathematically it is not possible to set up pure standing waves in the presence of longitudinal flow. However, the observationally detected flows are very slow, almost 10% of the local Alfvén speed; as a result, a quasi-standing pattern may be formed. Under such a situation the dominant temporal part of equation (15) can be approximated as given in Terradas, Goossens, and Ballai (2010a) as

$$\cos(\omega_f t) + \cos(\omega_b t) = 2\cos\left(\frac{\omega_f + \omega_b}{2} t\right)\cos\left(\frac{\omega_f - \omega_b}{2} t\right), \quad (16)$$

where

$$\omega_{av} = \frac{\omega_f + \omega_b}{2} = k c_k \sqrt{1 - \frac{\rho_{01}\rho_{02}}{(\rho_{01}+\rho_{02})^2}\frac{U^2}{c_k^2}} \quad (17)$$

and

$$\Delta\omega = \frac{\omega_f - \omega_b}{2} = \frac{\rho_{02}}{(\rho_{01}+\rho_{02})} kU. \quad (18)$$

The above equation (16) clearly visualizes that the loop is oscillating with an average frequency (ω_{av}), and is modulated by an envelope that oscillates with a "beat" frequency of $\Delta\omega$. This is an important modification of standing waves introduced by flow, which can be exploited for the observations of Ofman and Wang (2008) of weakly attenuated kink oscillations in the presence of background flow. In strong damped oscillations, where waves are damped within the periods of one to two, as for example oscillations detected by the EUV telescope aboard the Transition Region and Coronal Explorer (TRACE) (e.g., Aschwanden et al. 1999; Schrijver et al. 2002), the beating frequency can be considered to be very low (i.e., very large envelope), corresponding to the observed slow flow speed of $\sim 10\%$ of the local Alfvén speed. This means that for all practical puposes the behaviour of the system is equivalent to standing waves, as proposed by Terradas, Goossens, and Ballai (2010a). It is also noted that the average frequency of the standing waves in the presence of flow [cf. equation (17)] is always less than the frequency of the static case (e.g., kc_k).

3.2. *Identification of the Observed Period in the Parameter Space of Density Contrast and Magnetic Field*

In figure 2, we show a contour plot of the period as a function of the density contrast and the magnetic field. Panel (a) of this figure corresponds to our disperison relation (1), while panel (b) correponds to a solution obtained by using a linear approximation of it i.e., equation (9) originally derived by Terradas, Goossens, and Ballai (2010a) [e.g., see their equation (17)]. From their equation (17), the period can be approximated as $2\pi/\omega_{av}$, with $\omega_{av} = (\omega_{kf+} + \omega_{kf-})/2$. We can see a very good agreement between the solution corresponding to our dispersion relation (1) and its counterpart linear approximate relation, derived by Terradas, Goossens, and Ballai (2010a). The observed period is labeled on both contour maps. It is very clear that the period is relatively more sensitive to the density contrast, as compared to the magnetic field. This can be justified because a large range of magnetic fields between 30 G and 50 G requires a range of density contrast of between 2 and 6. From this figure it is apparent that there may be an infinite number of possible equilibrium combinations of the magnetic field and the density contrast to achieve the observed period in the parameter space of the density contrast and the magnetic field. In other words we can say there is no constraint to bound the range of these parameters. This is where we can apply a beating phenomenon and the associated modulating time as an additional parameter to constrain the values of the density contrast and the magnetic field corresponding to the range of observed flows.

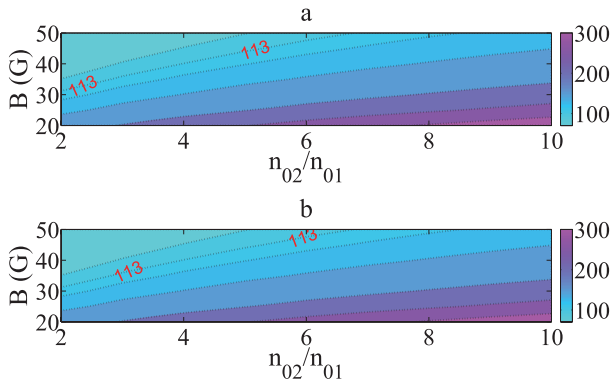

Fig. 2. Variation of the period as a function of the density contrast ratio and the magnetic field; (a) from dispersion relation (1), and (b) from a linear approximation of it given by Terradas, Goossens, and Ballai (2010a). The observed period, 113 s, is indicated on the plots.

3.3. *Modulating Time of the Standing Waves as a New Diagnostic*

First we shall emphasize the reason for denoting the time corresponding to the quarter-beat period wave as a modulating time. As can be seen, the modulating signal, or beat wave within the "quarter-beat period approximation", contains only one wave train, like the attenuating signal; its amplitude also varies with time. Hence, to apply a similar terminology we represent the time corresponding to the modulating signal when its amplitude becomes zero as a modulating time. As we know, there are obvious differences between the modulating and attenuating signals; especially, the context of envelopes attained by them is noteworthy. For a comparison point of view, within one wavetrain approximation, we take the attenuation time by following the standard definition of the "e-folding" envelope, i.e., the time when the amplitude of the signal becomes $1/e$ of the initial value. However, for the modulating signal or beat wave, we take the modulating time when the signal amplitude becomes zero, because its amplitude varies as a "cosine" function, thereby known as a "cosine-folding" envelope. Please recall that in the context of a beat wave we are considering only one wavetrain that lies within the the quarter period of a beat envelope to compare with observed attenuating signal. We are biased to do this because the present

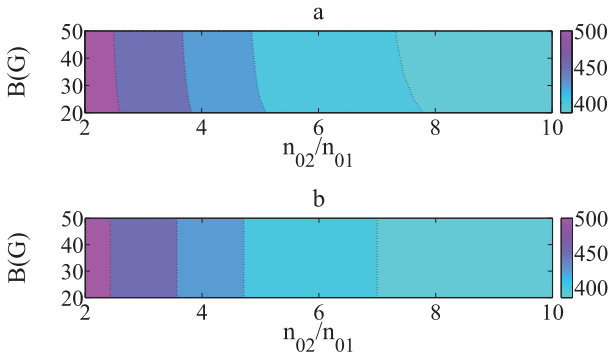

Fig. 3. Modulating time as a function of the density contrast ratio and the magnetic field corresponding to a flow of $\sim 100\,\mathrm{km\,s^{-1}}$, which lies well within the range of the observed flows of Ofman and Wang (2008). (a) corresponds to the solution of the dispersion relation (1), and (b) corresponds to its linear counterpart given by Terradas, Goossens, and Ballai (2010a).

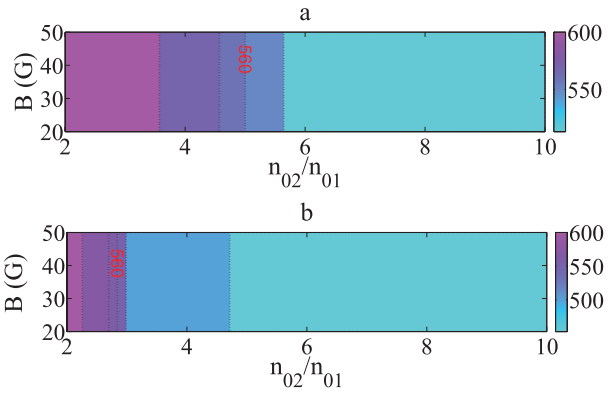

Fig. 4. Modulating time as a function of the density contrast ratio and the magnetic field corresponding to two different flows, (a) $75\,\mathrm{km\,s^{-1}}$ and (b) $85\,\mathrm{km\,s^{-1}}$, which lies well within the range of the observed flows of Ofman and Wang (2008). The modulating time equal to the observed damping time (560 s) is indicated on the plots.

observation does not exist for more than the quarter period of a beat wave.

In figure 3 we show a contour plot of the modulating time (i.e., τ_{m}) as a function of the density contrast and the magnetic field for a flow of $100\,\mathrm{km\,s^{-1}}$. Panel (a) of this figure corresponds to our dispersion relation (1), whereas panel (b) corresponds to a linear analytical relation derived under the assumption of slow flow by Terradas, Goossens, and Ballai (2010a). A slight deviation in the iso-modulating curves can be seen in these two panels that is obvious because panel (a) corresponds to the full dispersion relation, while panel (b) corresponds to its linear approximation. We can see that the modulating time is a good diagnostic of the density contrast. The modulating time varies more rapidly for low values of the density contrast, as compared to the high values of the density contrast. Observations clearly showed standing oscillations with weak damping of the damping time around 560 s, i.e., the amplitude of the standing waves becomes $1/e$ of the initial amplitude during that time. We consider this damping time as a reference time to examine whether beating due to flows modulates the amplitude of the standing waves before this time, or not. It is noted that for the beat frequency, $\Delta\omega = 0.003\,\mathrm{s^{-1}}$, corresponding to a flow of $100\,\mathrm{km\,s^{-1}}$, the beat period is $2\pi/\Delta\omega = 2094\,\mathrm{s}$, and therefore many wavetrains corresponding to the observed signal of period 113 s can be seen during a beat period. However, observations are available for a very short time around the 3 periods of oscillations, because threads where these observations were detected are present in the loops only up to that time. Hence, this restricts us to consider only one wavetrain due to modulation for a comparison with an observation that lies within one quarter of the beat-period envelope. We also noticed that for flow on the order of $100\,\mathrm{km\,s^{-1}}$, the modulating time is always shorter than the observed damping time, 560 s, which manifests that the amplitude of the standing waves would become zero before the observed damping time. However, such a pattern has not been observed, and the envelope of the signal seems to be dominated by attenuation rather than the modulation, i.e., $\tau_{\mathrm{D}} < \tau_{\mathrm{m}}$. Hence, we can anticipate that the observed value of the flows would be in a lower range (i.e., $75 < U < 100\,\mathrm{km\,s^{-1}}$) of the observed flows.

To justify this in figures 4a and 4b, we again show the modulating time in parameter space of the density contrast and the magnetic field for two different values of flows, 75 and $85\,\mathrm{km\,s^{-1}}$, respectively, using the linear approximate relation (7) originally derived by Terradas, Goossens, and Ballai (2010a). We notice that the modulating time of the standing wave is almost independent of the magnetic field. Further, by increasing the value of flow from $75\,\mathrm{km\,s^{-1}}$ to $85\,\mathrm{km\,s^{-1}}$ the iso-modulating curves, which satisfy the criterion $\tau_{\mathrm{m}} \geq \tau_{\mathrm{D}}$ are found to be shifted toward the lower values of the density contrast. Therefore, in order to find a more appropriate range of the density contrast corresponding to the lower range ($\leq 100\,\mathrm{km\,s^{-1}}$) of the observed flows, we again plot iso-modulating time curves in figure 5 in the parameter space of the density contrast and flow for a magnetic field of 30 G. Since it is evident that the modulating time is almost independent of the magnetic field, figure 5 would be almost the same for any arbitrary value of the magnetic field. From this figure we can see that the inequality $\tau_{\mathrm{m}} \geq \tau_{\mathrm{D}}$, required for the observed damped signal, would be satisfied when the density contrast exists between 2 and 5, and the associated flow will exist between 75 and $92\,\mathrm{km\,s^{-1}}$, corresponding to the observed flow in the range 74–$123\,\mathrm{km\,s^{-1}}$. Hence, we find that for a given value of flow, the inequality $\tau_{\mathrm{m}} \geq \tau_{\mathrm{D}}$ imposes an upper limit for the density contrast. As a result, corresponding to this value of the density contrast, we can predict a maximum value of the magnetic field through iso-period curves (cf. figure 2).

As an example, an inspection of figure 2 along with figure 5 reveals that for a given observed flow of $85\,\mathrm{km\,s^{-1}}$ a density contrast of ≈ 3 and a magnetic field of about 35 G for the thread seems to be quite consistent with the observations. This value of the magnetic field is 1.75-times larger than the value of the magnetic field of 20 ± 7 G, predicted by Ofman and Wang (2008). This discrepancy can be explained simply in terms of the different values of the density contrast used between these two calculations. At a low value of the density contrast, equating the kink speed with the phase speed yields $B = 2L\sqrt{2\pi(\rho_{01} + \rho_{02})}/P$ (Van Doorsselaere et al. 2008b), a useful relation for calculating the value of the magnetic field.

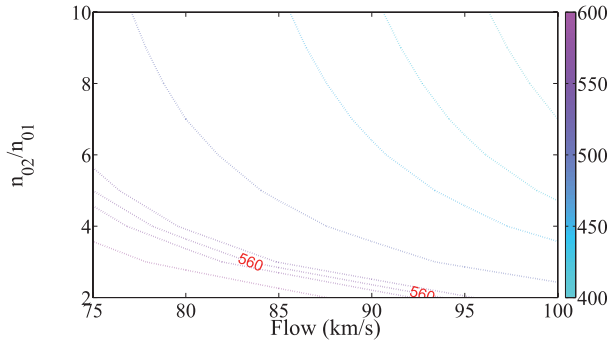

Fig. 5. Modulating time as a function of the flow and the density contrast ratio for the coronal loop thread of a magnetic field of 30 G. The modulating time equal to the observed damping time (560 s) is marked on plot.

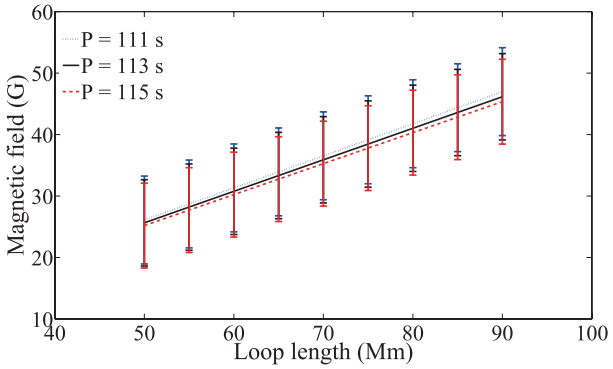

Fig. 6. Error bars in estimating the magnetic field as a function of the loop length corresponding to three different time periods using the cylinder model of the loop.

However, Ofman and Wang (2008) used the approximate relation $B = 2L\sqrt{2\pi\rho_{02}}/P$ in their calculation, which is valid at very high values of the density contrast ratio ($\rho_{02} \gg \rho_{01}$). That is not our case, however; our calculation corresponds to a low-density contrast ratio. We also show error bars in the estimation of the magnetic field as a function of the loop length for three different time periods, taking into account the value of the density contarst, 3, as shown in figure 6. The different time periods correspond to the uncertainty in the measurement of the observational period, i.e., $P = 113 \pm 2$ s.

3.4. Damping of Standing Waves due to Resonance Absorption in the Presence of Longitudinal Flow

As mentioned above, the flow splits the damping rate of the standing waves, which means that the forward wave of the standing wave attains a different damping rate, as compared to the backward wave. Consequently, we can say that it is not possible to determine a unique value of the damping rate for the standing waves in the presence of flow, as is generally considered for determining the damping rate in the absence of flows, i.e., an "e-folding" exponential damping. We can see from equation (10) that for a given flow the damping rate is defined by three unknown parameters, namely the magnetic field, density contrast ratio, and radial inhomogeneity length scale, if we replace the kink frequency in terms of the observed loop length (i.e., $\omega_k = \pi c_k/L$). However, when we replace the kink frequency in terms of the observed period, i.e., $\omega_k = 2\pi/P$, as given in Ruderman and Roberts (2002), the damping rate can be expressed only in terms of two unknown parameters, namely the density contrast ratio and the radial inhomogeneity length scale. We now discuss the behaviour of the damping time in these two ways separately. First, we consider the behaviour of the damping time in terms of three unknown parameters. In order to do that, we fix one unkown parameter for a specific value, and then analyze the damping time in the parameter space of the other two unknown quantities.

As an example, let us see the variation in the damping time as a function of the density contrast and the magnetic field for both the forward and backward waves of the standing waves, while keeping the inhomogeneity length scale at a fixed value, as shown in figures 7 and 8 (cf. panels a and c of these figures). We have taken the value of flow speed to be on the order of 85 km s^{-1}. A close inspection of figures 7 and 8 shows that due to this splitting, the contour line corresponding to the observed damping time is shifted upward for the forward wave and downward for the backward wave, as compared to the static case (cf. panel b of these figures) in the parameter space of the density contrast and the magnetic field. Besides this, we also note that for a fixed value of the radial inhomogeneity length scale, the damping time is found to be relatively more sensitive in the context of the higher values of the magnetic field and lower values of the density contrast; otherwise, it becomes almost flat parallel to the density contrast axis. We can further see from figures 7 and 8 that a reducion in the value of l/R by a factor 2 needs an equal factor increment in the value of the magnetic field to achieve the same damping rate. Hence, we can say that the observed damping time in the parameter space of the magnetic field and the density contrast can be easily tuned to higher or lower values of the magnetic field by varying the inhomogeneity length scale. Figure 9 shows behaviour of the damping time as a function of the magnetic field and the radial inhomogeneity length scale for a specified value of the density contrast, 3, and flow of 85 km s^{-1}. Panel (a) of this figure corresponds to the forward wave of the standing wave, while panel (c) corresponds to the backward wave. The damping time associated with the static case, i.e., when the flow is zero, is shown in panel (b) of this figure. The required damping time for the forward wave always corresponds to higher values of the magnetic field and the radial inhomogeneity length scale, as compared to the backward wave of the standing wave. That means even a precise measurement of the magnetic field and the density contarst, as discussed above, for example 35 G of the magnetic field and the density contrast 3 would lead to a few percent ($\sim$8%–10%) uncertainty in the estimation of the radial inhomogeneity length scale.

We now switch towards the second way of defining the damping time, as discussed above, which means expressing the kink frequency, ω_k, in equation (10) in terms of the observed period, P, as adopted earlier by Ruderman and Roberts (2002). This way of defining the kink frequency reduces the parameter space of three unknown quantities, namely the density contrast, radial inhomogeneity length scale, and magnetic field

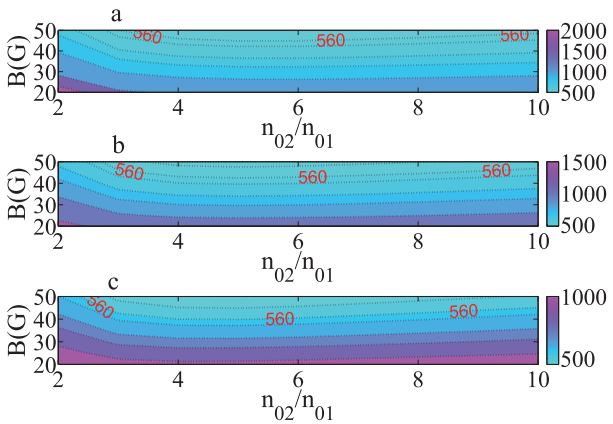

Fig. 7. Damping time as a function of the density contrast ratio and the magnetic field for the two waves: (a) forward and (c) backward, corresponding to flow of $\sim 85\,\mathrm{km\,s^{-1}}$ and $l/R = 0.2$. The damping time corresponding to no flow, consequently, no splitting, is given in (b). The observed damping time is labeled on the plots.

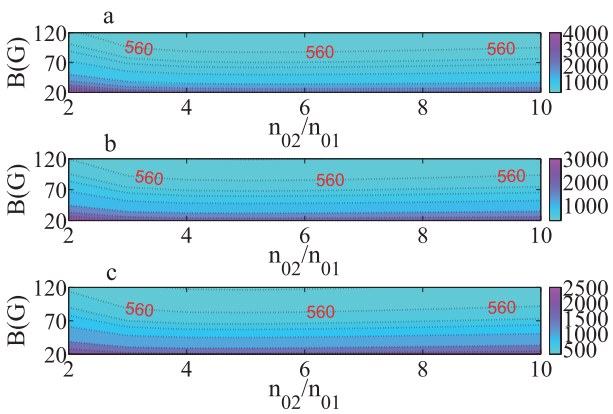

Fig. 8. Same as figure 7, but for $l/R = 0.1$.

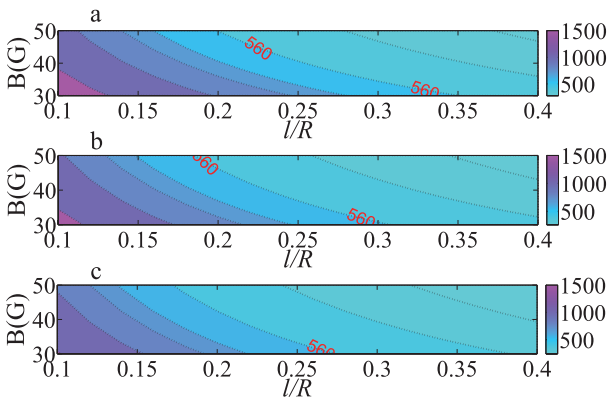

Fig. 9. Curves of the constant damping time as a function of the magnetic field and of the radial inhomogeneity scale length ratio, l/R, for a density contrast ratio of 3 and a flow of $85\,\mathrm{km\,s^{-1}}$ for the two waves: (a) forward and (c) backward. The damping time corresponding to no flow, and consequently no splitting, is given in panel (b). The observed damping time is labeled on the plots.

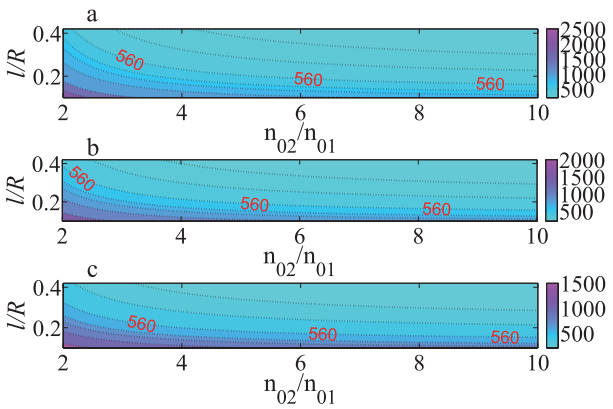

Fig. 10. Curves of the constant damping time as a function of the density contrast and the radial inhomogeneity length scale for the two waves (i.e., panels a and c correspond to forward and backward waves, respectively) for a flow speed of $85\,\mathrm{km\,s^{-1}}$ and a wave period of 113 s. The damping time corresponding to no flow, consequently, no splitting, is depicted in panel (b). The observed damping time is labeled on the plots.

to two unknown quantities of the density contrast and the radial inhomogeneity length scale, which means that it reduces the additional requirement of the magnetic field. In figure 10 we present curves of the constant damping time in the parameter space of the density contrast and the radial inhomogeneity length scale for both the forward and backward waves of the standing wave [panels (a) and (c)]. Panel (b) corresponds to the case when there is no flow, and consequently no splitting in the damping time of the standing waves. We have again taken the value of the flow speed to be $85\,\mathrm{km\,s^{-1}}$ and a period of $P = 113\,\mathrm{s}$, corresponding to the observed value. We again justify that the flow is shifting the location of the observed damping time upward for forward and downward for the backward waves of the standing waves in the parameter space of the density contrast and the radial inhomogeneity length scale, as compared to the location corresponding to the situation with no flow. In order to clarify more the uncertainty in the measurement of the radial inhomogeneity length scale across the coronal loop radius, we further show the variation of the damping time as a function of the radial inhomogeneity length scale corresponding to the observed period of 113 s, as shown in figure 11. We have taken the value of the density contrast equal to be 3, as estimated earlier, and associated flow equal to be $85\,\mathrm{km\,s^{-1}}$. From this figure we can clearly see that the flow leads an $\sim 8\%$–10% uncertainty in the estimation of the radial inhomogeneity length scale across the loop boundary.

4. Discussion and Conclusions

In all applications of coronal seismology to date, the observed oscillation period and the damping time have been used as important diagnostics for measuring the coronal magnetic field and radial inhomogeneity length-scale. The effect of flow has been studied in detail (Nakariakov & Roberts 1995); further, Joarder, Nakariakov, and Roberts (1997) noticed that high-speed steady flow of the order of the phase speed of the wave can lead to negative energy wave instabilities. However, none of the studies gave any importance to the flow for speeds much smaller than the phase speeds of the

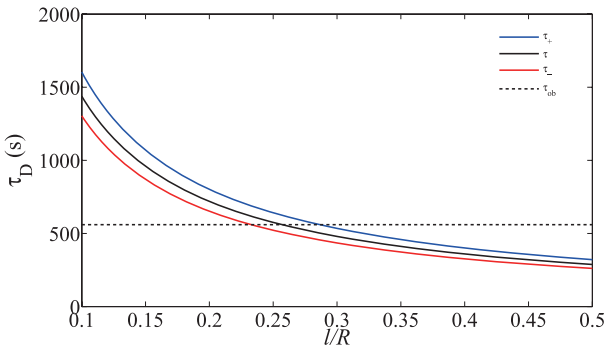

Fig. 11. Variation of the damping time as a function of the radial inhomogeneity length scale for a density contrast of 3, a flow of 85 km s^{-1}, and an observed period of 113 s. The observed damping time, 560 s, is indicated by a dashed horizontal line.

waves. In addition, Gruszecki, Murawski, and Ofman (2008) showed that slow flow enhances the damping of the oscillations, while Terradas, Goossens, and Ballai (2010a) showed that a small value of flow can produce beating of the standing waves. What we have clearly demonstrated in this paper is that small flows of the order of the observation of Ofman and Wang (2008), produce beating as well as splitting in the damping time due to resonant absorption of the standing kink wave in the coronal loop. The inherent properties of these two waves are totally different; beat waves arise due to a change in the real part of the frequency by flow, whereas attenuation caused by resonance absorption occurs due to the imaginary part of the complex frequency, as a result of mode conversion at the inhomogeneous layer of the loop boundary. Moreover, the envelope of the beat wave attains an oscillatory "cosine-folding" pattern that oscillates with a so-called beat period, rather than an "*e*-folding" non-oscillatory envelope, attained by resonance absorption. If the observations are long lasting, viz., in the context of the present observation, which is under discussion, we can say that if threads had been presented in the loop for a complete beat period (e.g., $\sim$2094 s corresponding to flow 100 km s^{-1}), these two phenomena could have been easily discriminated, just by counting the number of wave trains, since the beat wave would be accomplished by many wave trains instead of a single wave train that leads by attenuation due to resonance absorption. However, in the limited period of observation that is available only up to a very short time, not more than a quarter of a beat period, we would be able to see only one wavetrain corresponding to the beat wave, too. Hence, it cannot be easily distinguished that the observed signals are modulated or attenuated ones. Therefore, in such a class of observation, an intriguing issue would be to find out whether the observed signal, i.e., a pattern of the wave amplitude variation with time, is modulated by flow, or attenuated by resonance absorption. For large values of the observed flows greater than 100 km s^{-1}, we find that the envelope of the beat wave is more effective and revealing the dominating character over the damped envelope until the period of observational existence. Since observations do not show such a dominated beating pattern, hence we can predict that the values of the flow must be in a lower range of the observed values, i.e., < 100 km s^{-1}. We find that the values in the range of 75–92 km s^{-1} only satisfy the criterion $\tau_m \geq \tau_D$, which seems to be compatible with the observational finding of the weak damping of a standing wave. Further, by searching in the parameter space of the density contrast versus the magnetic field, we have clearly constrained the density contrast to be about 3, while the magnetic field is very firmly determined to be close to 35 G for a flow of 85 km s^{-1}, which lies well within the range of 75–92 km s^{-1}, with the cylinder being the preferred shape for the coronal loops. This value is somewhat different from the estimate of 20 ± 7 G obtained by Ofman and Wang (2008); this discrepancy can be resolved in terms of a different choice of the density contrast ratio. Our solution corresponds to low-density contrast, instead of high-density contrast chosen by Ofman and Wang (2008).

In recent years, the phenomenon of resonance absorption has come to know as a most promising mechanism for explaining the damping of transverse kink oscillations in coronal loops. We have noted that in the presence of flow damping time of standing waves splits, and it corresponds to two different values corresponding to forward and backward waves, instead of having a common value. As a result, we cannot precisely estimate the value of the radial inhomogeneity length-scale across the loop boundary, even after a precise estimation of the magnetic field and the density contrast. Viz., a flow of 85 km s^{-1} yields $\sim$8%–10% uncertainty in the estimation of the radial inhomogeneity length scale for a magnetic field of 35 G and a density contrast of 3, as discussed above in subsection 3.4.

Thus, as a concluding remark, we can say that field-aligned flows do have important consequences for observations of standing waves in coronal structures. On one hand, it produces the phenomenon of beating, and a comparison of beat wave within "quarter beat-period approximation" with attenuating waves provides an upper bound for the density contrast in the parameter space of the density contrast and the flow. This upper bound of the density contrast further helps in estimating the upper bound of the magnetic field through the iso-period curve in the parameter space of the magnetic field and the density contrast corresponding to the observed value of the period. On the other hand, the flow splits the damping rates of the standing waves, which leads an uncertainty in estimating the radial inhomogeneity length scale across the loop boundary.

We sincerely thank the anonymous referee for his/her valuable comments and suggestions. This work was partly supported by WCU grant No. R31-10016 from the Korean Ministry of Education, Science and Technology. One of the authors (T. M.) was also supported by Basic Science Research Program (2010-0009258, PI: T. Magara) through the National Research Foundation of Korea.

References

Antia, H. M., Basu, S., & Chitre, S. M. 2008, ApJ, 681, 680
Aschwanden, M. J., Fletcher, L., Schrijver, C. J., & Alexander, D. 1999, ApJ, 520, 880
Basu, S., Antia, H. M., & Tripathy, S. C. 1999, ApJ, 512, 458
Edwin, P. M., & Roberts, B. 1983, Sol. Phys., 88, 179
Goossens, M., Arregui, I., Ballester, J. L., & Wang, T. J. 2008, A&A, 484, 851
Goossens, M., Hollweg, J. V., & Sakurai, T. 1992, Sol. Phys., 138, 233
Gruszecki, M., Murawski, K., & Ofman, L. 2008, A&A, 488, 757
Hollweg, J. V., Yang, G., Cadez, V. M., & Gakovic, B. 1990, ApJ, 349, 335
Joarder, P. S., Nakariakov, V. M., & Roberts, B. 1997, Sol. Phys., 176, 285
Nakariakov, V. M., Ofman, L., DeLuca, E. E., Roberts, B., & Davila, J. M. 1999, Science, 285, 862
Nakariakov, V. M., & Roberts, B. 1995, Sol. Phys., 159, 213
Nakariakov, V. M., Roberts, B., & Mann, G. 1996, A&A, 311, 311
Narayanan, A. S. 1990, Nuovo Cimento D, 12, 1491
Narayanan, A. S. 1991, Plasma Phys. Controlled Fusion, 33, 333
Ofman, L. 2007, ApJ, 655, 1134
Ofman, L., & Wang, T. 2002, ApJ, 580, L85
Ofman, L., & Wang, T. J. 2008, A&A, 482, L9
Roberts, B., Edwin, P. M., & Benz, A. O. 1984, ApJ, 279, 857
Ruderman, M. S., & Roberts, B. 2002, ApJ, 577, 475
Schrijver, C. J., Aschwanden, M. J., & Title, A. M. 2002, Sol. Phys., 206, 69
Terradas, J., Goossens, M., & Ballai, I. 2010a, A&A, 515, A46
Terradas, J., Goossens, M., & Verth, G. 2010b, A&A, 524, A23
Thompson, M. J., et al. 1996, Science, 272, 1300
Tomczyk, S., McIntosh, S. W., Keil, S. L., Judge, P. G., Schad, T., Seeley, D. H., & Edmondson, J. 2007, Science, 317, 1192
Uchida, Y. 1970, PASJ, 22, 341
Van Doorsselaere, T., Nakariakov, V. M., & Verwichte, E. 2007, A&A, 473, 959
Van Doorsselaere, T., Nakariakov, V. M., & Verwichte, E. 2008a, ApJ, 676, L73
Van Doorsselaere, T., Nakariakov, V. M., Young, P. R., & Verwichte, E. 2008b, A&A, 487, L17
Vasheghani Farahani, S., Van Doorsselaere, T., Verwichte, E., & Nakariakov, V. M. 2009, A&A, 498, L29
Verwichte, E., Nakariakov, V. M., Ofman, L., & Deluca, E. E. 2004, Sol. Phys., 223, 77
Wang, T., Innes, D. E., & Qiu, J. 2007, ApJ, 656, 598